Catalytic Study of Methanol-to-Olefins Conversion in Four Small-Pore Silicoaluminophosphate Molecular Sieves: Influence of the Structural Type, Nickel Incorporation, Nickel Location, and Nickel Concentration

Marie-Ange Djieugoue, A. M. Prakash, and Larry Kevan*

Department of Chemistry, University of Houston, Houston, Texas 77204-5641

Received: February 9, 2000

The selectivity of four small-pore silicoaluminophosphate molecular sieves, including SAPO-34 (CHA), SAPO-35 (LEV), SAPO-17 (ERI), and SAPO-18 (AEI), toward light olefins in general and ethylene in particular has been investigated for the methanol-to-olefins reaction using gas chromatography. This study was prompted by earlier electron spin resonance and electron spin−echo modulation results on nickel-modified SAPO materials in which Ni(I) was incorporated into both framework and ion-exchanged sites. These seemingly similar materials behaved significantly differently with respect to reducing agents and adsorbates. Attention was focused on whether the catalyst performance is influenced by the structural type, the presence of a transition metal ion (Ni) either in the framework or at ion-exchanged positions, or the amount of incorporated transition metal ion. Our results show that these factors indeed play an important role in the catalytic behavior. Among the protonated H−SAPO-*n* materials, the highest combined distribution of ethylene, propylene, and butenes (C_2−C_4 olefins) was obtained with H−SAPO-34, and the lowest with H−SAPO-35, which also had the shortest lifetime for catalytic activity. H−SAPO-18 turned out to be the best catalyst in terms of lifetime for catalytic activity. Incorporation of Ni(II) into the framework increased the lifetime, the overall distribution of C_2−C_4 olefins (in the case of NiAPSO-34), and the selectivity of the catalysts toward ethylene (in the cases of NiAPSO-34 and NiAPSO-18), whereas incorporation of Ni(II) by means of solid-state ion exchange (NiH−SAPO-*n*) increased only the selectivity toward ethylene. Also, the increase in ethylene selectivity was more prominent in synthesized than in ion-exchanged samples. Among the Ni-loaded samples, NiAPSO-34 was found to be the best catalyst in terms of both ethylene selectivity and lifetime, whereas NiH−SAPO-18 exhibited the worst ethylene yield and NiH−SAPO-35 the shortest lifetime. Finally, the effect of the amount of Ni was investigated in NiAPSO-34. It appears that the selectivity toward ethylene does not increase linearly with NiAPSO samples prepared with an increasing amount of Ni in the reaction gel. In fact, there seems to be an optimum Ni concentration for which ethylene selectivity reaches a maximum and above which ethylene selectivity decreases. This optimum concentration is the same as was found in earlier studies to yield the strongest Ni(I) signal, as observed by ESR.

Introduction

Light olefins are key components in the petrochemical industry and will likely play a dominant role in any future methanol-based chemical economy. Conventionally, they are produced by thermal cracking of naphtha consisting of C_5−C_{12} alkanes. Methanol, which can be produced readily from coal or natural gas via synthesis gas ($CO + H_2$) by existing and proven technologies, offers an interesting alternative.[1] Although methanol itself is a potential motor fuel and can be blended with gasoline, it would require large investments to overcome the technical problems associated with its use. Mobil's zeolite-based process for the conversion of methanol to gasoline provided a new route for the conversion of coal to gasoline.[2] The importance of light olefins as intermediates in the conversion of methanol to gasoline has prompted several studies on methods for selectively producing them from methanol on zeolite catalysts. The development of silicoaluminophosphate molecular sieves with microporous framework structures offers other interesting perspectives.

Molecular sieves with pore openings of about 0.45 nm show very interesting shape-selectivity properties for the conversion of methanol to olefins (MTO process).[3] They can only sorb straight-chain molecules such as primary alcohols and linear paraffins and olefins, but not branched isomers and aromatics. The pore opening is smaller than the kinetic diameter of branched and aromatic molecules, but large enough to permit the access of linear molecules. Their pore openings are eight-membered oxygen rings whose dimensions vary with the shape of the rings, which can be circular or puckered and elliptical, but the effective size is always smaller than 0.45 nm. The porous systems of small-pore molecular sieves are formed by ellipsoidal or spherical cavities that share the eight-membered oxygen rings to generate a three-dimensional channel system. These cages are generally much larger than the connecting windows.

Silicoaluminophosphates (SAPOs) are a new generation of crystalline microporous molecular sieves.[4] They are synthesized by incorporating Si into the framework of the aluminophosphate (AlPO) molecular sieves. The present study focuses on four SAPOs: erionite-like SAPO-17, chabazite-like SAPO-34, levyne-like SAPO-35, and SAPO-18, whose structure is closely related to, but crystallographically distinct from, that of SAPO-34. Whereas chabazite and erionite have strong acid sites in their protonic form, the corresponding SAPO's show mild to moderate acidity.[3] Also, in SAPO materials, the concentration of

10.1021/jp000504j CCC: $19.00
Published on Web 06/17/2000

TABLE 1: Gel Compositions for SAPO-34, NiAPSO-34, SAPO-35, SAPO-17, SAPO-18, and NiAPSO-18

catalyst	gel composition
SAPO-34	Al_2O_3:P_2O_5:SiO_2:R_1[a]:H_2O = 1.0:1.0:0.6:2:60
NiAPSO-34	NiO:Al_2O_3:P_2O_5:SiO_2:R_1[a]:H_2O = 0.03:0.985:1.0:0.6:2:60
SAPO-35	Al_2O_3:P_2O_5:SiO_2:R_2[b]:H_2O = 1.0:1.0:0.3:1.5:55
SAPO-17	Al_2O_3:P_2O_5:SiO_2:R_3[c]:H_2O = 1.0:1.0:0.1:1.0:60
SAPO-18	SiO_2:Al_2O_3:P_2O_5:R_4[d]:H_2O = 0.3:1.0:0.92:1.6:50
NiAPSO-18	NiO:SiO_2:Al_2O_3:P_2O_5:R_4[d]:H_2O = 0.03:0.3:1.0:0.92:1.6:50

[a] R_1 stands for morpholine. [b] R_2 stands for hexamethyleneimine. [c] R_3 stands for cyclohexylamine. [d] R_4 stands for *N*,*N*-diisopropylethylamine.

Brønsted acid sites increases with the Si/Al ratio.[3] This may be explained by the assumption that a SAPO material is obtained by silicon substitution into an ideal aluminophosphate framework. The predominant mechanism appears to be silicon substitution for phosphorus, but it is also possible that substitution of two silicons for an aluminum−phosphorus pair takes place.[4] The first mechanism leads to SAPO materials having frameworks with a net negative charge that are balanced by a protonated template in the as-synthesized form and by protons in the calcined form. Thus, the acidity of SAPO materials depends on the structure type, the Si/Al ratio, and the specific mechanism of silicon substitution.

In this study, we report how the performance of four small-pore SAPO catalysts in the MTO process is influenced by their framework structure, the incorporation of a transition metal ion (Ni), and the location (framework or extraframework site) and concentration of this ion. We also try to correlate these results to those of our previous studies in which the nature and adsorbate interactions of nickel in some of these materials were studied using electron spin resonance (ESR) and electron spin−echo modulation (ESEM) spectroscopies.

Experimental Section

Synthesis. The detailed preparations of the SAPO-34, NiAPSO-34, NiH−SAPO-34, SAPO-35, NiH−SAPO-35, SAPO-17, and NiH−SAPO-17 materials are described in the cited references.[5] To obtain a highly crystalline and pure SAPO-17 phase, it was necessary to use a relatively small concentration of silicon in the synthesis gel. Synthesis of NiAPSO-18 was accomplished as follows. About 20 g of water were added to 7.3 g of Catapal B alumina, and the mixture was stirred for 2 h. Then, 10.6 g of phosphoric acid, 0.4 g of nickel acetate, and 20 g of water were added to the initial solution over a 10-min period, and the resulting mixture was stirred for 2 h until homogeneous. The next step consisted in adding 0.9 g of silica and 1.2 g of water to the previous mixture, stirring for 30 min, and then adding 10.3 g of templating agent, *N*,*N*-diisopropylethylamine. A gel was formed by stirring the final reaction mixture vigorously for 2 h. This gel, with a pH of 6.2, was sealed in a Teflon-lined stainless steel autoclave and heated at 165 °C under autogenous pressure for 8 days. The solid product was recovered by filtration, washed with distilled water, and dried. Synthesis of SAPO-18 is achieved following the same route but omitting the step for addition of the nickel source. The gel compositions of the reaction mixtures are summarized in Table 1. The organic template trapped within the micropores of the as-synthesized solids was removed by calcination in flowing air at 823 K for 16 h prior to catalyst testing.

Sample Treatment and Measurements. Product purity was first verified by X-ray diffraction. Powder X-ray diffraction (XRD) patterns were recorded on a Siemens D5000 X-ray diffractometer using Cu Kα radiation. Product purity was also verified by elemental analysis. Chemical analysis of the samples was performed by electron microprobe analysis with a JEOL JXA-8600 Electron Beam Superprobe operated at a beam voltage of 15 kV and a current of 30 nA. Si and O were calibrated with diopsite, $CaMgSi_2O_6$; Ni with metallic Ni; Al with anorthite, $CaAl_2Si_2O_8$; and P with monazite. Prior to measurement, the samples were prepared as pressed pellets to make a dense material with a reasonably smooth surface. The electron beam was defocused to 10 μm in diameter to minimize the damage caused to the specimen by heating. Data were collected from 3−5 randomly chosen regions and averaged to represent the bulk composition. The precision was usually <1% for all elements, and the accuracy is estimated at ±2−3% for cations and ±5% for oxygen.

Catalyst Testing. The calcined samples were pelletized and then crushed to particles prior to being sieved. Then, 0.2 g of sieved sample with a particle size between 150 and 180 μm was loaded in a tubular quartz reactor with a 10-mm internal diameter. The catalysts were activated at 460 °C under a 10 mL/min nitrogen flow overnight. The catalysts were tested at 400 °C. The products were analyzed by on-line gas chromatography with a Varian 3300 gas chromatograph equipped with a flame ionization detector and a capillary column to separate the C_1−C_4 hydrocarbons. The weight hourly space velocity (WHSV) was 0.5 h^{-1}. The injection was completed in 10 seconds. The products were first analyzed after 10 minutes of reaction time on stream and then every hour to allow for complete stabilization of the gas chromatograph. Selectivities are expressed as molar percentages. Retention times and response factors were determined by using a standard gas mixture calibration. Regeneration of the catalysts was achieved by calcination in air at 803 K overnight.

Results

X-ray Powder Diffraction (XRD). Figure 1 shows the powder XRD patterns of SAPO-34, SAPO-35, SAPO-17, and SAPO-18 in their as-synthesized form. These patterns match, both in intensity and line position, the patterns reported for the corresponding structure types 34, 35, 17, and 18. The structure of SAPO-17 is made up of a hexagonal unit cell with lattice parameters $a = b = 13.23$ Å, $c = 14.77$ Å, and $\gamma = 120°$. The unit cell parameters in SAPO-18 are $a = 13.72$ Å, $b = 12.74$ Å, $c = 18.60$ Å, and $\beta = 90°$. SAPO-34 has unit cell parameters $a = b = 13.2$ Å, $c = 15.1$ Å. SAPO-35 has rhombohedral symmetry with unit cell parameters $a = b = c = 10.75$ Å, $\alpha = \beta = \gamma = 76° 25'$. Practically no loss in crystallinity was observed when the as-synthesized SAPO-34, -35, and -17 samples were heated to 823 K for 16 h to remove the organic templates. However, Chen et al. reported that significant changes in XRD patterns occurred upon going from the as-synthesized form to the calcined form of SAPO-18.[6] They stressed that, for the as-synthesized samples, peaks in the SAPO-18 patterns are observed in addition to those of as-synthesized AlPO-18 (for example, at $2\theta = 16.0°$, d spacing = 5.6 Å). Upon gentle dehydration at a temperature at which the template remains intact (e.g., 125 °C), the corresponding SAPO-18 pattern changes to closely resemble that of the monophasic calcined, dehydrated series of AlPO-18 and SAPO-18 samples. They also mentioned the fact that an as-synthesized SAPO-18 pattern can be considered as two superimposed patterns that closely correspond to those for as-synthesized AlPO-18 and calcined, dehydrated AlPO-18. The presence of two different crystallographic forms in one SAPO-18 sample was interpreted as an inhomogeneity in the distribution of silicon within a single framework structure. Synthesized NiAPSO-34 and NiAPSO-18 exhibit patterns similar to those of the corresponding SAPOs.

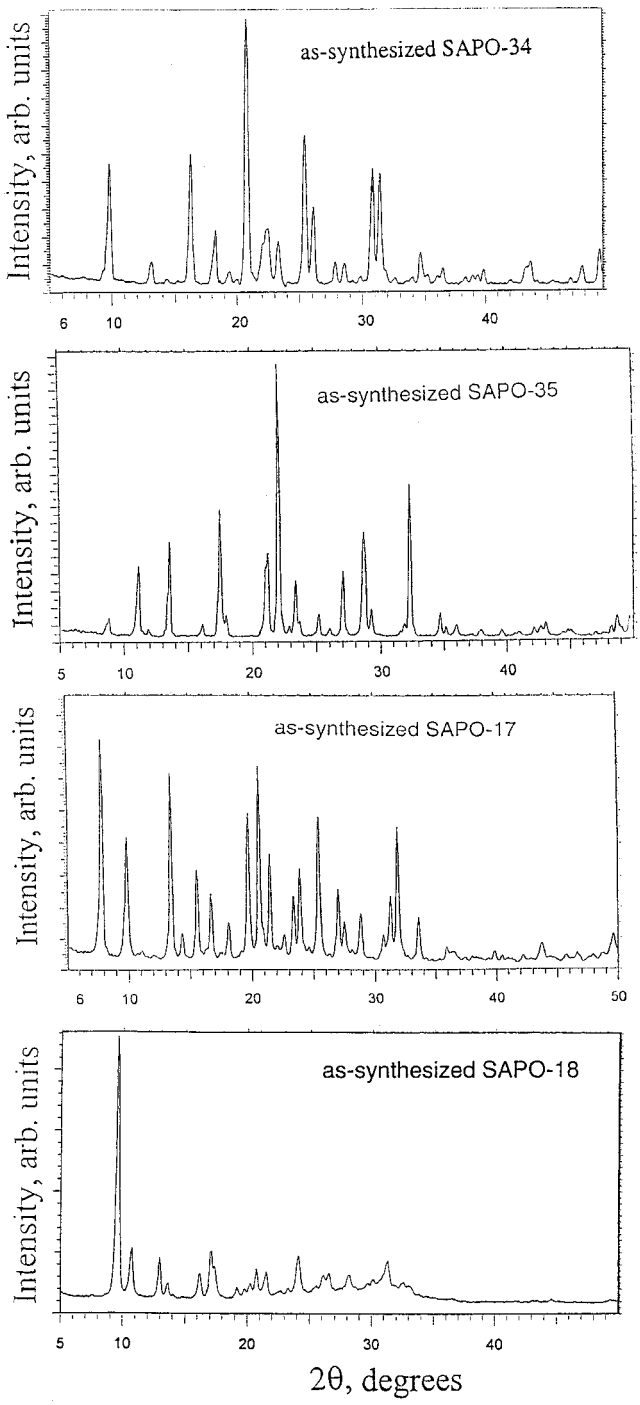

Figure 1. X-ray powder diffraction patterns of as-synthesized (a) SAPO-34, (b) SAPO-35, (c) SAPO-17, and (d) SAPO-18.

Electron Microprobe Analysis. The chemical composition of the samples was estimated by electron microprobe analysis. Except for the SAPO-18 samples, no significant differences were seen between the regions, which indicates a uniform elemental composition over the samples. For SAPO-18 samples, some particles were found to be Si-rich while others were found to be Si-poor. For these samples, the values were averaged over a large number of particles for a particular sample. The results are given in Table 2. The observed framework chemical composition for SAPO-34, -35, and -17 suggests isolated Si-atom substitution for P. In SAPO-17 samples of low silicon content, it has been reported that the content of P_2O_5 decreases proportionally with increasing SiO_2 content, whereas the Al_2O_3 content is practically constant.[7] This also supports isolated

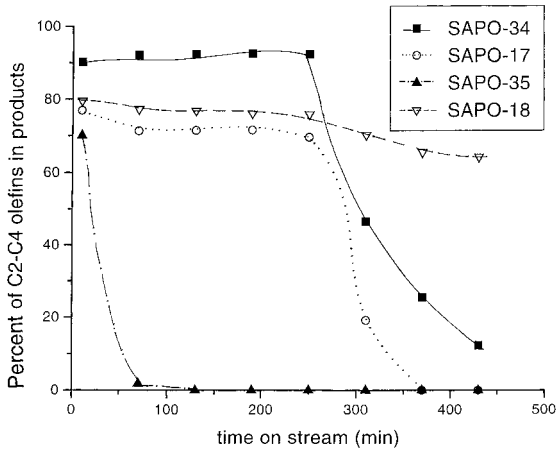

Figure 2. Percent of C_2-C_4 olefins in the total products from methanol as a function of time on stream for SAPO-34, SAPO-35, SAPO-17, and SAPO-18.

TABLE 2: Elemental Analysis and Si/(Si + Al + P) Ratios for SAPO-34, NiH−SAPO-34, NiAPSO-34, SAPO-35, NiH−SAPO-35, SAPO-17, NiH−SAPO-17, SAPO-18, NiH−SAPO-18, and NiAPSO-18

catalyst	elemental analysis	Si/(Si + Al + P)
SAPO-34	$(Si_{0.155}Al_{0.498}P_{0.348})O_2$	0.155
NiH−SAPO-34	$(Ni_{0.003}Si_{0.155}Al_{0.498}P_{0.345})O_2$	0.155
NiAPSO-34	$(Ni_{0.004}Si_{0.132}Al_{0.491}P_{0.373})O_2$	0.132
SAPO-35	$(Si_{0.06}Al_{0.5}P_{0.44})O_2$	0.06
NiH−SAPO-35	$(Ni_{0.003}Si_{0.06}Al_{0.05}P_{0.437})O_2$	0.06
SAPO-17	$(Si_{0.02}Al_{0.5}P_{0.483})O_2$	0.02
NiH−SAPO-17	$(Ni_{0.003}Si_{0.02}Al_{0.05}P_{0.48})O_2$	0.02
SAPO-18	$(Si_{0.09}Al_{0.498}P_{0.32})O_2$	0.087
NiH−SAPO-18	$(Ni_{0.003}Si_{0.09}Al_{0.498}P_{0.317})O_2$	0.087
NiAPSO-18	$(Ni_{0.004}Si_{0.07}Al_{0.498}P_{0.343})O_2$	0.07

silicon substitution for P and has been confirmed independently by ^{29}Si MAS NMR.[8] In SAPO-18, it is known that Si substitutes for both Al and P, the amount of substituted P being larger than that of substituted Al.[6]

Catalyst Testing. *(1) Influence of the Structural Type*. In addition to ethylene and propylene, which are the main reaction products, butenes and methane were also detected. The catalysts turned brown and later gray during the reaction. Figure 2 shows the percent of C_2-C_4 olefins in the products as a function of the time on stream (TOS) for calcined SAPO-34, SAPO-35, SAPO-17, and SAPO-18 at 400 °C. All of the SAPOs under investigation convert methanol to C_2-C_4 olefins at the given temperature, but the selectivity and lifetime of the samples vary significantly. For a time on stream between 10 and 250 min, SAPO-34 exhibits the highest selectivity toward C_2-C_4 olefins (maximum near 92%), followed by SAPO-18 (∼80%), and SAPO-17 (∼78%). When the time on stream exceeds 250 min, the selectivities of SAPO-34 and SAPO-17 decrease dramatically, reaching 10% for SAPO-34 and 0% for SAPO-17 at TOS = 430 min. On the other hand, the selectivity of SAPO-18 decreases only slightly and is still quite high (∼65%) at TOS = 430 min. The behavior of SAPO-35 is completely different from that of the other samples. Although initially its selectivity is similar to that of SAPO-18 and SAPO-17 (∼70% at TOS = 10 min), it decreases very quickly to reach 2% at TOS = 70 min. In summary, the selectivity toward C2−C4 olefins decreases in the order SAPO-34 > SAPO-18 > SAPO-17 ≫ SAPO-35 for TOS < 250 min and in the order SAPO-18 > SAPO-34 > SAPO-17 ≫ SAPO-35 for TOS > 250 min. Also, the lifetime of the catalysts decreases in the order SAPO-18 > SAPO-17 > SAPO-34 ≫ SAPO-35, whereas their deactivation

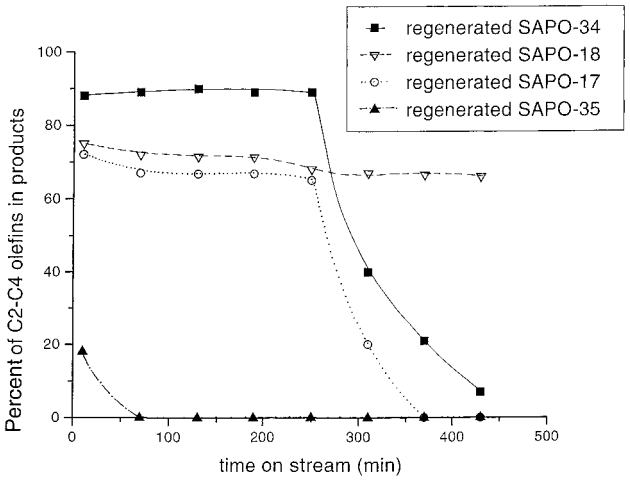

Figure 3. Percent of C_2-C_4 olefins in the total products from methanol as a function of time on stream for regenerated SAPO-34, SAPO-35, SAPO-17, and SAPO-18.

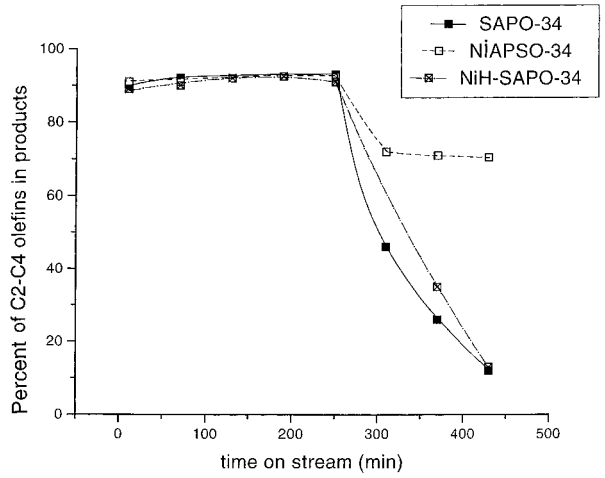

Figure 4. Percent of C_2-C_4 olefins in the total products from methanol as a function of time on stream for SAPO-34, NiAPSO-34, and NiH−SAPO-34.

rate (slope of the distribution of olefins as a function of the time on stream) decreases in the order SAPO-35 ≫ SAPO-17 > SAPO-34 > SAPO-18. Figure 3 shows the percent of C_2-C_4 olefins in the products as a function of the time on stream for "regenerated" SAPO-34, SAPO-35, SAPO-17, and SAPO-18. For SAPO-34, SAPO-35, and SAPO-18, the regenerated samples exhibit selectivities that are an average of 4% below those of the original samples. However, regenerated SAPO-35 has a selectivity of only 16% compared to 70% for the original sample at TOS = 10 min.

(2) Influence of Ni Incorporation and Location. Figure 4 shows a comparative plot of the percent of C_2-C_4 olefins in the products as a function of the time on stream for SAPO-34, NiAPSO-34, and NiH−SAPO-34. The behavior of SAPO-34 has already been described in Figure 2. The selectivity of NiH−SAPO-34 is basically the same as that of SAPO-34 throughout the time range, except at TOS = 250 min and TOS = 370 min for which the selectivity of NiH−SAPO-34 is about 10% higher than that of SAPO-34. As for NiAPSO-34, for TOS < 250 min, its selectivity is also the same as that of SAPO-34, and then it decays from 92% to reach a plateau at 70%. A plot of the selectivity to C_2-C_4 olefins as a function of TOS for SAPO-17 and NiH−SAPO-17 is shown in Figure 5. The two samples exhibit almost the same trend. A similar plot of the selectivities

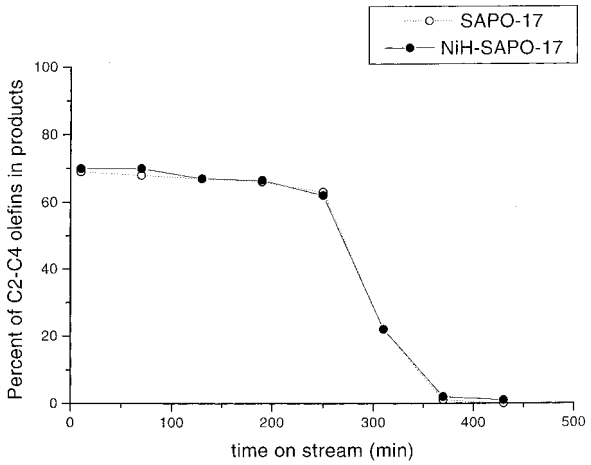

Figure 5. Percent of C_2-C_4 olefins in the total products from methanol as a function of time on stream for SAPO-17 and NiH−SAPO-17.

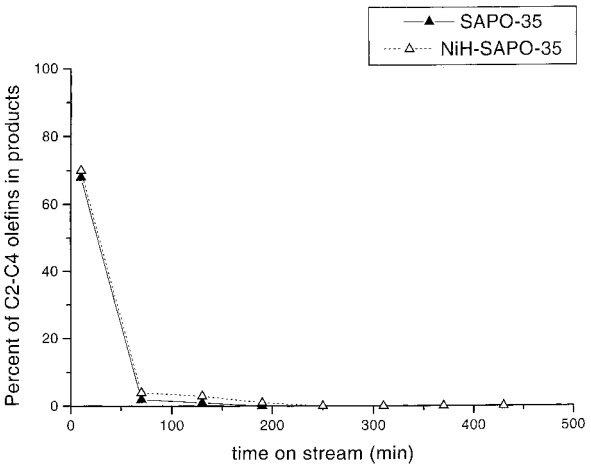

Figure 6. Percent of C_2-C_4 olefins in the total products from methanol as a function of time on stream for SAPO-35 and NiH−SAPO-35.

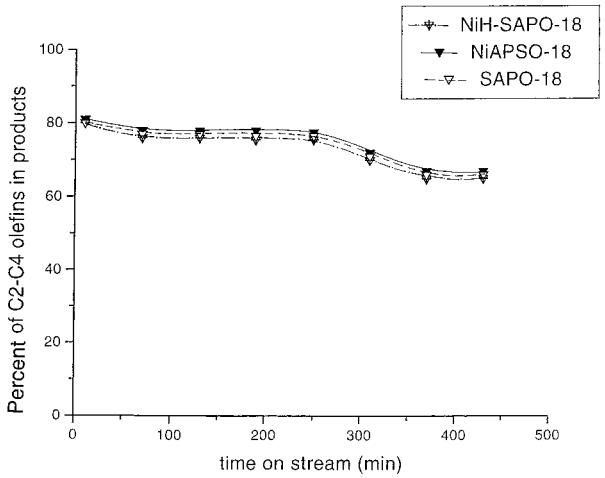

Figure 7. Percent of C_2-C_4 olefins in the total products from methanol as a function of time on stream for SAPO-18, NiAPSO-18, and NiH−SAPO-18.

to C_2-C_4 olefins is shown in Figure 6 for SAPO-35 and NiH−SAPO-35. The results are almost identical for the two samples. Finally, Figure 7 also gives identical patterns for SAPO-18, NiAPSO-18, and NiH−SAPO-18. With the hope of gaining a better understanding of the effect of Ni incorporation, we plotted ethylene selectivity as a function of TOS for all of the samples. The results are shown in Figures 8−11. Figure 8 shows that,

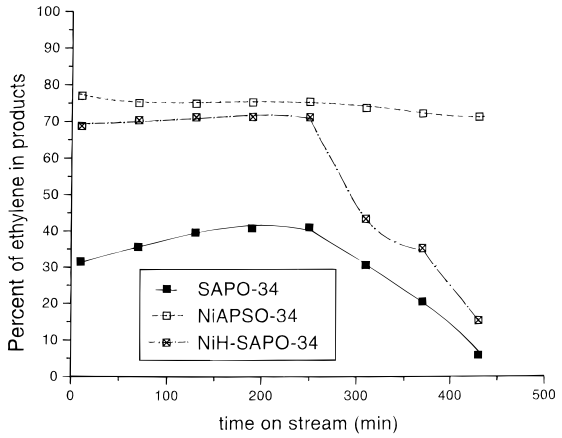

Figure 8. Percent of ethylene in the total products from methanol as a function of time on stream for SAPO-34, NiAPSO-34, and NiH−SAPO-34.

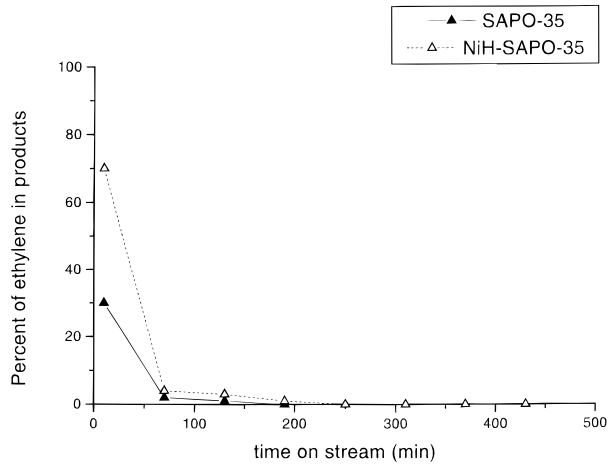

Figure 9. Percent of ethylene in the total products from methanol as a function of time on stream for SAPO-35 and NiH−SAPO-35.

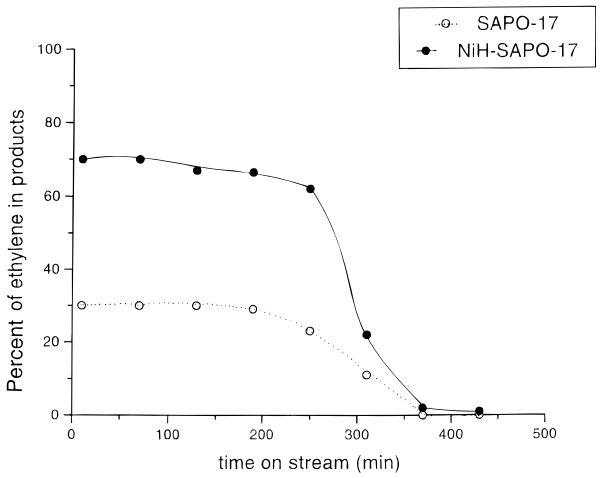

Figure 10. Percent of ethylene in the total products from methanol as a function of time on stream for SAPO-17 and NiH−SAPO-17.

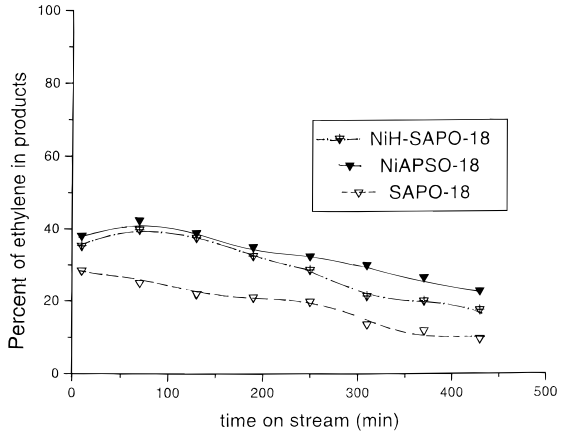

Figure 11. Percent of ethylene in the total products from methanol as a function of time on stream for SAPO-18, NiAPSO-18, and NiH−SAPO-18.

whereas the highest ethylene selectivity in SAPO-34 is ∼40% and is reached for TOS = 250 min, NiAPSO-34 and NiH−SAPO-34 show selectivities close to 80%. For SAPO-34, the selectivity toward ethylene increases slowly from ∼30% at TOS = 10 min to its maximum (40%) at TOS = 250 min and then decreases rapidly to reach 5% at TOS = 430 min. The sample in which Ni was incorporated into the extraframework sites of SAPO-34 (NiH−SAPO-34) follows a trend similar to that of SAPO-34. The selectivity to ethylene also increases slowly from 69% at TOS = 10 min to 71% at TOS = 250 min and then decreases rapidly when the time on stream is longer than 4 h to reach about 12% at TOS = 7 h. When Ni is incorporated into the synthesis gel of SAPO-34 (NiAPSO-34), the behavior is rather different from that of the two other samples. The selectivity attains its maximum in the early stages of the reaction (78% at TOS = 10 min), decreases slightly to 72% at TOS = 1 h, and then reaches a plateau (at TOS = 7 h, ethylene selectivity is still about 70%). Hence, NiAPSO-34 remains active for a much longer time than SAPO-34 and NiH−SAPO-34. Figure 9 shows that, for SAPO-35, the highest selectivity toward ethylene is only 30% and is reached at the beginning of the reaction (TOS = 10 min). After 1 h, no more ethylene can be detected in the products. Incorporating Ni into the extraframework sites of SAPO-35 increases the highest ethylene selectivity from 30% in SAPO-35 to 70% in NiH−SAPO-35 (TOS = 10 min). However, the same pattern as in SAPO-35 is also seen in NiH−SAPO-35 in the sense that ethylene selectivity decreases rapidly as the time on stream increases (∼0% at TOS = 1 h). Again, it is evident from Figure 10 that the incorporation of Ni into the extraframework positions of SAPO-17 causes a noticeable increase in the selectivity toward ethylene, especially for TOS < 250 min (the highest ethylene selectivity in SAPO-17 is 30%, whereas it is 70% in NiH−SAPO-17). For times on stream longer than 250 min, the distribution of ethylene in NiH−SAPO-17 is more or less the same as its distribution in SAPO-17. We can see from Figure 11 that the enhancement of ethylene selectivity caused by the incorporation of Ni either in framework or in extraframework positions of SAPO-18 is noticeable, but not as apparent as in the other cases. There is only about a 10% difference between the highest ethylene selectivity in SAPO-18 (30%) on one hand and NiH−SAPO-18 (40%) and NiAPSO-18 (42%) on the other hand. These values are also quite low compared to those obtained with the previous Ni catalysts, whose initial ethylene selectivities are in the 70−80% range. Also, the three samples follow a very similar pattern, and as the time on stream increases, not much decay occurs in the ethylene selectivity (the difference in ethylene selectivity between TOS = 10 min and TOS = 430 min is 18% for NiAPSO-18, 17% for NiH−SAPO-18, and 11% for SAPO-18).

(3) Influence of Ni Concentration. The influence of the Ni concentration was studied for the sample that exhibited the highest selectivity toward ethylene as well as the longest lifetime. That sample was found to be NiAPSO-34. Figure 12 shows the percent of ethylene in the products as a function of

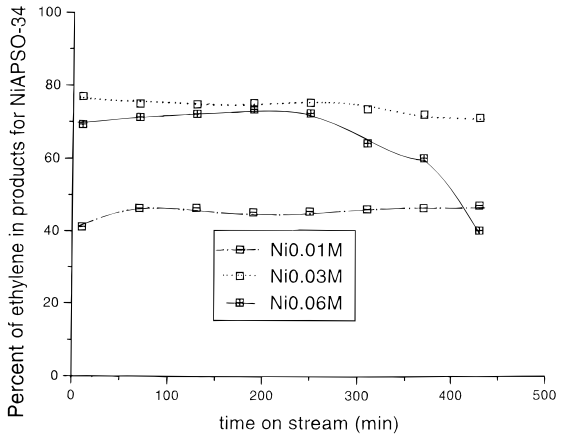

Figure 12. Percent of ethylene in the total products from methanol as a function of time on stream for NiAPSO-34 with [Ni] = 0.01 M, 0.03 M, and 0.06 M.

the time on stream for three NiAPSO-34 samples prepared with varying Ni concentrations of 0.01, 0.03, and 0.06 M in the synthesis gel. For [Ni] = 0.01 M, the selectivity toward ethylene increases slowly from 40 to 45% and then reaches a plateau. When the concentration of Ni is increased to 0.03 M, ethylene selectivity also increases, with a maximum around 78% and a plateau behavior, as has already been described in Figure 8. Unexpectedly, as the concentration of Ni is further increased to 0.06 M, the ethylene selectivity does not continue to increase also. For TOS < 250 min, the distribution of ethylene in the products is similar (though slightly less) than that for [Ni] = 0.03 M. For TOS > 250 min, the ethylene selectivity drops significantly and is only 40% after 7 h on stream.

Discussion

One of the most important features of zeolite catalysts is their ability to act as molecular sieves because their channels have molecular dimensions. Three types of shape selectivity can be distinguished: reactant, product, and restricted transition state selectivity, depending on whether reactants can enter into, products can leave from, or intermediates can be formed in the zeolite catalyst, respectively. The structures under investigation in this work have two main common characteristics. They are small-pore, cage-type molecular sieves. Reactivities, diffusivities, and most other properties of a homologous series usually change monotonically with the length of the molecule.[9] However, certain molecules in some molecular sieves do not obey this rule, i.e., their reactivity and diffusion behavior differ from those of their neighbors in the homologous series.[9] This is known as the cage or window effect. The three most important and interesting manifestations of the cage effect in cage-type zeolites are that (1) the variation of the diffusion coefficient versus the chain length shows a minimum at C_8 and a maximum at C_{12}; (2) hydrocracking rates of *n*-hexane, *n*-decane, and *n*-undecane are much higher than that of *n*-octane; and (3) *n*-C_7, *n*-C_8, and *n*-C_9 are missing from the cracked products of longer *n*-paraffins.[9]

These phenomena, which were mostly encountered in erionite, were explained as follows. The length of *n*-octane, which was found to be the paraffin to exhibit the lowest diffusion coefficient and hydrocracking rate, is 12.8 Å and fits almost exactly into the 13-Å cavity of erionite. Molecules in such tight-fitting cages have low mobility. Also, molecules longer than *n*-C_8 will not completely fit into one cage, and part of them will extend into the next cage. Their diffusitivity is thus enhanced compared to that of smaller molecules; *n*-dodecane, which is 17.6 Å long, extends across a unit cell in the *a* direction and is held by three eight-membered rings, which ensures maximum mobility. Reaction rates of *n*-paraffins in zeolites that exhibit the cage effect increase or decrease with chain length as their diffusivities increase or decrease. The product selectivity described in point (3) occurs because, once *n*-C_7, *n*-C_8, and *n*-C_9 form inside the cavities, they cannot get out until they are cracked to butanes by acid sites. Dodecane, on the other hand, can diffuse out of the cavity rapidly enough to remain intact.

The general reaction path of methanol conversion to hydrocarbons has been described in the literature as follows.[10]

$$2CH_3OH \underset{+H_2O}{\overset{-H_2O}{\rightleftharpoons}} CH_3OCH_3 \xrightarrow{-H_2O} C_2{=}C_3{=} \rightarrow \begin{matrix}\text{isoparaffins}\\ \text{aromatics}\\ C_6^+\ \text{olefins}\end{matrix}$$

It is agreed that methanol is first dehydrated to dimethyl ether, which has been shown to be an unstable primary product.[11] The equilibrium mixture is then converted to light olefins, which are stable secondary products. In the final steps of the process, the C_2-C_5 olefins are converted to paraffins, aromatics, naphthenes, and higher olefins by polycondensation and alkylation reactions. Olefin production is favored by higher reaction temperatures, shorter contact times, lower acidity catalysts, and lower pressures.[12] Small-pore zeolites such as erionite can be used to produce ethylene in high yield, although this reaction is always accompanied by rapid deactivation by coke.[12] The methanol-to-olefins process is fairly exothermic (~49 kJ/mol) and has been demonstrated in a fluid-bed process at a scale of 100 barrels/d (16 m^3/d).[9] Union Carbide disclosed a new MTO catalyst based on silicoaluminophosphate materials.[4] The SAPO catalyst reportedly produces olefins in very high yields (>90%) with no aromatics. The major problem of methanol conversion is to obtain higher selectivity of C_2-C_4 olefins compared to higher olefins, which can be obtained via catalyst modification or by reaction in the presence of excess steam. These help in suppressing the autocatalytic step in some manner. Our results show that several factors can influence the activity and selectivity of MTO catalysts.

(1) Effect of the Structural Type. SAPO-17, SAPO-18, SAPO-34, and SAPO-35 are all cage-type small-pore molecular sieves having either circular or elliptical pore openings. SAPO-34 has rhombohedral symmetry. Its framework consists of double six-membered rings arranged in layers in the sequence ABCABC. The hexagonal prisms formed in this way are linked by tilted four-membered rings. The resulting framework possesses large, ellipsoidal cages. The cavities are interconnected to six others by puckered elliptical eight-membered rings (Figure 13). The main difference between SAPO-34 and SAPO-35 resides in the size of their cavities in the sense that the chabazite cage is made up of 12 four-membered rings, 2 six-membered rings, and 6 eight-membered rings, whereas the levyne cage is made up of 9 four-membered rings, 5 six-membered rings, and only 3 eight-membered rings. This makes the chabazite cage significantly larger than the levyne cage (Figure 13). Also, the circular pore opening in SAPO-34 has a free diameter of 3.8 × 3.8 Å. On the other hand, SAPO-35 has an elliptical window with a free diameter of 3.6 × 4.8 Å.

SAPO-18 is a crystallographically novel but chabazite-related aluminophosphate.[13] The window dimensions are same as those of SAPO-34 of 3.8 × 3.8 Å. The main structural difference between SAPO-18 and SAPO-34 resides in the orientation of the double six-membered ring units from which both are built. In SAPO-18, alternate layers of double six-membered rings

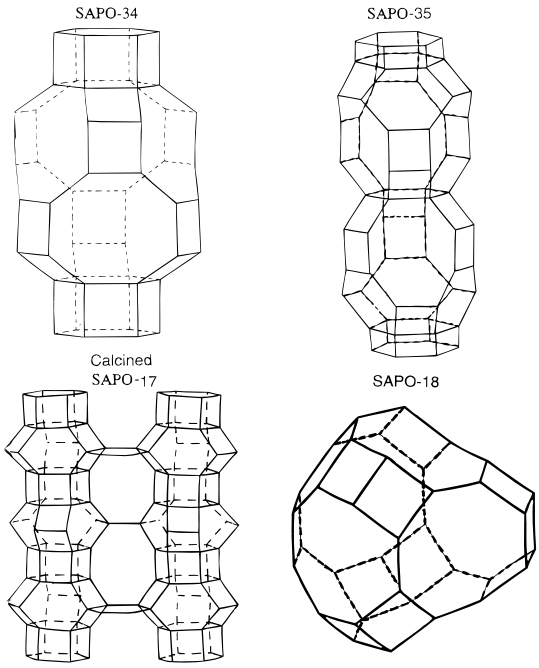

Figure 13. Cage structure for SAPO-34, SAPO-35, calcined SAPO-17, and SAPO-18.

parallel to the *ab* plane are related by a *c*-glide and thereby have different orientations. This causes the supercage formed between hexagonal prisms to have a pearlike shape (Figure 13). In SAPO-34, the layers are related by a simple translation and therefore have the same orientation. Because of this difference, the cages available in these two structures are significantly different from each other.

The main cage in SAPO-17, also known as an "erionite supercage", has dimensions 6.3 × 13 Å and is the largest of the four structures (Figure 13) as it is made up of 12 four-membered rings, 5 six-membered rings, and 6 eight-membered rings. SAPO-17 has hexagonal symmetry, and its framework consists of double six-membered ring units arranged in the sequence AABAAC. These hexagonal prisms are linked by four-membered rings and single six-membered rings (cancrinite cages). The supercages are supported by columns formed by cancrinite units and hexagonal prisms. The result is a complex pore system interconnected by eight-membered rings. Molecules have access to the main cavity through the six elliptical openings formed by eight-membered rings. The elliptical opening has a free diameter of 3.6 × 5.1 Å.

It is postulated that the primary requirement for catalytic activity is that the solid be acidic and be capable of forming carbonium ions by reaction with a hydrocarbon.[14] A description of acidity in general, and surface acidity more specifically, requires the determination of the nature, the strength, and the number of acid sites. It is also important to be able to distinguish between Brønsted acid sites (those able to transfer protons from the solid to the adsorbed molecule) and Lewis acid sites (those able to accept an electron pair from the adsorbed molecule). Infrared spectroscopic studies of ammonia adsorbed on solid surfaces have often been used to achieve this distinction and to assess the numbers of Brønsted and Lewis acid sites independently. For example, ammonia can adsorb on a surface physically as NH_3, it can be bonded to a Lewis acid site as coordinatively bound NH_3, or it can be adsorbed on a Brønsted acid site as NH_4^+. Each of these species is independently identifiable from its characteristic IR adsorption bands, allowing the number of Lewis and Brønsted acid sites on a surface to be determined quantitatively. Isomorphous substitution of silica into a microporous aluminophosphate creates a negative framework charge, allowing for the charge-balancing protons in the silicoaluminophosphate to act as Brønsted acid sites. That is the reason SAPOs can be used as solid acid catalysts. Temperature-programmed desorption of NH_3 was used to assess the strength and concentration of Brønsted acid sites in SAPO-34, -17, and -18.[15] The authors reported that the strength of Brønsted acid sites is in the order SAPO-17 < SAPO-18 < SAPO-34, based on their high-temperature desorption peaks, and that their concentrations are in the order SAPO-18 < SAPO-17 < SAPO-34, based on the intensity of their high-temperature desorption peaks. It has also been stressed that the selectivity to light olefins is enhanced when the Si/Al ratio is lowered, probably because of the reduction of the concentration of strong acid sites and because samples with lower Si/Al exhibit higher ethylene yield.[6] Of the four materials investigated, SAPO-17 has the lowest Si/Al ratio (∼0.04), whereas SAPO-34 contains the greatest amount of Si. It is therefore important to consider all of these factors when comparing the performance of the catalysts. Moreover, Wilson and Barger found that reducing the Si content increases the catalyst life.[16] They pointed out that, because of the variety of Si siting (isolated Si and Si islands) in SAPOs, there is no direct correlation between the Si content and the number of acid sites[17] but that, for SAPOs with low Si content, as is the case for SAPO-17, Si sites are often isolated and there is one acid site per Si.[18] It has also been reported that the presence of OH groups at 3600 cm^{-1}, which correspond to Al−OH bonds, greatly influences methanol conversion into hydrocarbons.[19] Consequently, it is very important that the access to these acid sites not be blocked. Thus, the strength and concentration of acid sites, along with the size and shape of the micropores in a SAPO catalyst, determine its activity, selectivity, and lifetime for an acid-catalyzed reaction.

Our results indicate that the performance of the catalysts is, indeed, greatly influenced by these factors. For the four structures, the cage size increases in the order SAPO-35 < SAPO-34 < SAPO-18 < SAPO-17. Our results show that, at the beginning of the reaction, SAPO-35 exhibits a high selectivity to C_2-C_4 olefins (70%) but, after only 1 h on stream, it almost completely loses its efficiency. Considering only pore geometry, as SAPO-35 has the smallest cage, its pores can be blocked by heavy secondary products such as coke more easily than the pores in the other SAPO structures, and this could explain, in part, why SAPO-35 is deactivated much more rapidly than the other three catalysts. Our results also show a slightly higher deactivation rate for SAPO-17, compared to that of SAPO-34, and a higher activity for SAPO-34. The differences in activities and deactivation rates among SAPO-17, SAPO-34, and SAPO-18, at least in the early stages of the reaction, can be explained mainly on the basis of the strength and the concentration of their acid sites. MAS NMR spectroscopy studies have shown that, in SAPO-34 synthesized in the presence of colloidal silica, Si substitutes only for P (mechanism I)[20] whereas, in SAPO-18, Si undergoes a dual substitution mechanism. In fact, in SAPO-18, Si can substitute not only via mechanism I (Si → P), but also via mechanism II (2Si → Al + P).[6] When substitution occurs through mechanism I, one Brønsted acid site is produced for every Si incorporated into the framework. On the other hand, substitution through mechanism II retains framework neutrality and therefore introduces no Brønsted acidity. Another study in which SAPO-34 was synthesized using morpholine as the templating agent and fumed

silica (Aerosil-200) as the Si source showed evidence from ^{29}-Si CP MAS NMR spectra that, in Si-poor SAPO-34 samples, Si substitutes via mechanism I whereas, in Si-rich samples, Si substitutes via both mechanisms I and II.[5a] In our study, SAPO-34 was synthesized using the method reported by the above authors, and the Si content was quite high [Si/(Si + Al + P) = 0.155]. We can therefore assume that, in our SAPO-34 sample, Si undergoes a dual substitution mechanism even though the majority of the silicon probably enters the framework via mechanism I. Such observations have also been reported for Si-rich SAPO-37 and SAPO-20 molecular sieves.[21] In SAPO-17, silicon substitutes only for phosphorus. Judging from their respective Si/(Si + Al + P) ratios, 0.02 for SAPO-17, 0.087 for SAPO-18, and 0.155 for SAPO-34, it is reasonable to say that the concentration of acid sites in the three catalysts is in the order SAPO-34 > SAPO-18 > SAPO-17. TPD of NH_3 spectra reported by Chen et al.[15] corroborate those reported by Prakash et al.,[5a] showing that acid sites in SAPO-34 are much stronger than those in SAPO-18 and SAPO-17. It appears that, for SAPO-17, SAPO-18, and SAPO-34, coke does not play a significant role in the early stages of the reaction (TOS < 250 min). During this stage, the performance of the catalysts strictly depends on the number and strength of the acid sites, to which it is directly proportional. However, as the time on stream increases, the effect of coke can no longer be overlooked. As more coke is formed, the pores start to become clogged. It has been observed that the higher the number of acid sites, the higher the rate of coke formation in the cavities.[22] This explains why SAPO-34 is deactivated more rapidly than SAPO-18. In fact, Chen et al. compared the activity and selectivity of SAPO-18 samples with Si/(Si + Al + P) ratios varying from 0 to 0.095 to that of SAPO-34 with Si/(Si + Al + P) = 0.1.[6] They found that SAPO-18 samples with high Si/(Si + Al + P) ratios retain their catalytic activity for a longer reaction time on stream than those with low Si/(Si + Al + P) ratios. Moreover, they corroborated our results by pointing out that the catalytic activity of SAPO-34, which has twice as many Brønsted acid sites as the most acidic (in terms of both number and strength of acid sites) SAPO-18 sample, drops off more rapidly than that of the latter.

On the other hand, the behavior of SAPO-17 compared to that of SAPO-18 for TOS > 250 min appears to be more complex. In fact, accounting for the fact that, although SAPO-17 has a lower Si content, it deactivates faster than SAPO-18 does not seem straightforward. In another study, Chen and co-workers observed that, at 500 °C, a SAPO-17 sample with Si/(Si + Al + P) = 0.05 is deactivated very rapidly and loses its activity within 20 min.[15] They explained this by stating that the accessible cages in SAPO-17 are much larger than those in in SAPO-18 and SAPO-34 and that, as a result, the transition state for coke is easier to form in SAPO-17. Because our experimental conditions were quite different from theirs, we cannot properly compare our results, although the results are somewhat consistent at least in terms of the deactivation rate of SAPO-17 being higher than that of SAPO-18. We believe that the particular behavior of SAPO-18 is somewhat linked to its particular geometry.

Despite the high selectivity for linear C_2-C_4 hydrocarbons, small-pore molecular sieves generally suffer from relatively rapid deactivation during methanol conversion, as illustrated by our results. The big cavities, which can be blocked by coke, are partly responsible for this phenomenon. Aromatics and heavy, branched compounds can be formed inside the large cages at high temperatures (e.g., 400 °C). These molecules are too big to diffuse through the porous structure. Thus, they remain inside the big cages, where they can form carbonaceous deposits blocking the pores and preventing the access of reagents to the active sites. In principle, the rate of deactivation increases with the catalyst acidity, given that all other factors are identical. Deactivation by coke may be due to both the covering of acid sites and the blockage of pore structure.[23] The interconnecting three-dimensional network of pores with supercages existing in small-pore molecular sieves provides room for accommodating some coke without immediately blocking the pores. It has been suggested that the deactivation by coke and its effect on the product distribution depend on the way in which the coke is deposited on the catalyst.[19] Initially, aromatics and branched isomers formed inside the cavity are adsorbed irreversibly on the strong acid sites. As a consequence, the concentration of strong acid sites decreases, and so does the olefin conversion to parafins. Subsequently, the pores are blocked, and the concentration of acid sites decays abruptly. The methanol conversion then drops. In this final stage, the principal products have been reported to be dimethyl ether (DME), methane, and small amounts of C_2-C_3 olefins, which are formed by reactions requiring only weak acid sites. In our results, DME was not observed, as is sometimes the case at high temperature. A study of the role of coke deposition in the conversion of MeOH to olefins over SAPO-34 defined this process as being a transition-state-shape-selective reaction.[11] It revealed that the coke formed from oxygenates, referred to as active coke, promoted olefin formation, whereas the coke formed from olefins, referred to as inactive coke, only had a deactivating effect. The yield of olefins during the MTO reaction was found to go to the formation of olefins, particularly ethylene. Another interesting result was that the ethylene-to-propylene ratio increased with the intracrystalline coke content, regardless of the nature of the coke.

Most catalysts can be totally or partially regenerated after being calcined in air at high temperature (803 K), as was observed in this study. However, except for a small loss in crystallinity during the regeneration process, we were not able to fully understand the reason that SAPO-34, SAPO-17, and SAPO-18 regained almost full activity whereas SAPO-35 suffered an appreciable deterioration. One possible reason may be the incomplete removal of coke by calcination at 803 K in SAPO-35. A permament loss of activity has been observed in cation-exchanged chabazites and attributed to structural degradation during regeneration.[24] Irreversible deactivation has also been observed in clinoptilolite samples modified by either ammonium ion exchange or hydrochloric acid treatment.[25] Gubisch and Bandermann found that, in HCl-exchanged zeolite Na-T, the catalyst activity decreased slowly with the number of regenerative cycles, independently of the regeneration temperature, and after 16 regenerations, the conversion of methanol dropped from 100% to 80%.[26]

(2) Effect of Ni Incorporation. It is quite apparent from our experimental results that nickel substitution into the SAPO-34 framework greatly increases its selectivity toward ethylene as well as its lifetime. The increase in the overall selectivity toward C_2-C_4 olefins is only observed for TOS > 250 min. In SAPO-34, it is known that Ni preferentially substitutes at a P site. This is also supported by the chemical analysis data, which suggest that no extraframework nickel cations are present in NiAPSO-34 (0.03 M). The framework negative charge is thus compensated for solely by protons, which are available for acid catalysis. The difference in selectivity toward ethylene between SAPO-34 and NiAPSO-34 cannot be attributed to a structure modifica-

tion due to the incorporation of nickel because the XRD patterns of the two materials are almost identical. Diffuse reflectance infrared Fourier transform spectroscopy of calcined NiAPSO-34 has been reported to show O−H stretching bands more intense than those of H^+−SAPO-34.[27] This led to the conclusion that the nickel-loaded catalyst has a higher density of acid sites than the Ni-free one. An NH_3 TPD study has also revealed that the acidity of NiAPSO-34 is weaker than that of its parent SAPO and is just sufficient for dehydration of DME.[28] The authors concluded that this must be responsible for the highly selective ethylene synthesis. NiAPSO-34's catalytic activity and selectivity are thus seen to be associated with the modification of the acidity of the molecular sieve by nickel. In fact, EXAFS analyses conducted by Thomas et al. have indicated that the nickel is incorporated into the structure with a large perturbation of the local environment and have also suggested the presence of a second extraframework coordination sphere, which, from infrared spectroscopy, seems to involve hydrogen bonding.[27] This has been thought to stabilize the local structure around nickel, which is believed to be shielded by the bridging species observed by EXAFS and DRIFTS.

Incorporation of Ni in the SAPO materials via solid-state ion exchange has little effect on the overall selectivity toward C_2−C_4 olefins but enhances the selectivity toward ethylene, especially in the early stages of the reaction (TOS < 250 min). It appears that, for the SAPO-34 series at short TOS, the method of incorporation of Ni does not really affect the performance of the catalyst, as the selectivity to C_2−C_4 olefins as well as to ethylene is roughly the same for NiAPSO-34 and NiH−SAPO-34. The method of incorporation only comes into play for longer reaction times, when the synthesized sample remains active while the ion-exchanged sample activity decays more rapidly and behaves basically like a Ni-free sample. Therefore, it appears that incorporation of Ni into framework sites, in addition to increasing ethylene selectivity, also makes the catalyst more resistant to deactivation caused by coke formation, whereas incorporation of Ni into extraframework sites only affects the ethylene yield. The increase in selectivity and lifetime in NiAPSO-34 materials supposedly containing nickel in the framework sites vs NiH−SAPO-34 materials containing nickel in ion-exchange sites is most probably due to the location of the active nickel(I) center. It should be noted that similar behavior has also been observed in Ni-loaded SAPO-5 and SAPO-11, which were tested as catalysts for ethylene dimerization.[29] In a framework site, Ni(I) is less accessible to large butenes, and therefore, oligomerization to hexenes and cracking is suppressed. In a sample in which the active Ni cations are in ion-exchanged sites, Ni(I) can be reduced by ethylene or butenes to metallic nickel clusters more easily than it can be reduced in a sample in which Ni is believed to be at framework sites and, therefore, less accessible to reducing agents. Our present results support our earlier electron spin resonance results in which, upon adsorption of ethylene on Ni(I) in NiH−SAPO-34, an ESR spectrum with a broad baseline was produced, clearly showing that some of the Ni(I) had been reduced to Ni(0). This phenomenon, however, was not observed in NiAPSO-34. Furthermore, our electron spin−echo modulation studies showed that, in NiH−SAPO-34, Ni is located at a site that corresponds to the center of a six-membered ring window displaced inside the chabazite cage. Such a site can be easily blocked by coke formation, and this can explain why Ni in NiH−SAPO-34 has the ability, like Ni in NiAPSO-34, to increase the ethylene selectivity at short TOS thanks to modified acidity but loses that ability at TOS > 250 min once coke formation becomes important.

It is still unclear, however, why incorporating Ni into SAPO-18 has so little effect on its performance and also why the SAPO-18 series exhibits an overall selectivity to C_2−C_4 olefins that is comparable to that of the other three SAPOs but has a lower selectivity for ethylene. This is perhaps related to the geometry of the material in some way.

(3) Influence of Ni Concentration. The results show that the selectivity toward ethylene increases as the Ni concentration is increased from 0.01 to 0.03 M but decreases as the concentration goes from 0.03 to 0.06 M, implying that there is an optimum Ni concentration for obtaining the best results. At higher Ni concentrations ([Ni] > 0.03 M), it is probably not possible to incorporate all of the Ni into the framework. Therefore, while some of it goes into the framework, part of it goes into extraframework positions. The combined effect of the framework and extraframework Ni when [Ni] = 0.06 M is probably responsible for the behavior observed in Figure 12, which is most noticeable for TOS > 250 min. This behavior can be thought of as being a compromise between the plateau expected for NiAPSO-34 and the rapid decay observed for NiH−SAPO-34 (Figure 8).

Conclusions

Most of the small-pore silicoaluminophosphates under investigation have been extensively studied in the past, for they have relatively strong Brønsted acid sites and exhibit shape-selectivity properties for the conversion of methanol to light hydrocarbons. However, except for a few authors who studied the activity of Ni−SAPO-*n* catalysts, where $n = 5$, 11, and 34,[27−29] to our knowledge, no report has been made on the performance of Ni−SAPO-*n* catalysts where $n = 17$, 18, or 35 for the MTO reaction. Among the four samples investigated in their protonated form, SAPO-34 was found to have the highest selectivity toward C_2−C_4 olefins (∼92%), whereas SAPO-35 had the lowest yield for C_2−C_4 olefins (∼70%) and the shortest lifetime. It was found that, although a higher number and strength of acid sites yield a better performance initially, in the long run, they lead to faster deactivation. This was shown by the fact that the performance of SAPO-34, with more acid sites than SAPO-18, decays much more rapidly than that of the latter, which led to the conclusion that SAPO-18 is the best catalyst among the four structures investigated in terms of lifetime for the MTO reaction. Except for SAPO-35, which could not be successfully regenerated by recalcination, all of the samples regained their activity and exhibited selectivities similar to fresh samples. The incorporation of Ni into the structures generally increased the ethylene yield, and among the Ni-containing samples, NiAPSO-34 proved to have the best performance in terms of both selectivity and lifetime. NiAPSO-*n* samples appeared to be generally better catalysts than NiH−SAPO-*n* samples. The increase in selectivity and/or lifetime for the formation of ethylene in NiAPSO-34 and NiAPSO-18 compared to NiH−SAPO-34 and NiH−SAPO-18 confirm our belief that a framework site has distinct catalytic advantages over an ion-exchange site.

Our results show a few discrepancies compared to some earlier reports. Because of the diversity of test conditions among various research groups evaluating catalytic activity for MeOH conversion to olefins, the experimental results often differ somewhat from group to group and make definitive catalyst comparisons difficult.

Acknowledgment. This research was supported by the National Science Foundation, the Robert A. Welch Foundation, and the Environmental Institute of Houston. The authors thank Zhidong Zhu for his extensive help in running the gas chromatography experiments.

References and Notes

(1) (a) Meisel, S. L.; McCullough, J. P.; Lechthaler, C. H.; Weisz, P. B. *Chemtech* **1976**, *2*, 86. (b) Wise, J. J.; Silvestri, A. J. *Oil Gas J.* **1976**, 140. (c) Gabelica, Z. In *Zeolites: Science and Technology*; Ribeiro, F. R., Rodrigues, A. E., Rollmann, L. D., Naccache, C., Eds.; Nijhoff: The Hague, The Netherlands, 1984; p 529.

(2) (a) Chang, C. D.; Silvestri, A. J.; Smith, R. L. U. S. Patent 3,894,-103, 1975. (b) Chang, C. D.; Silvestri, A. J.; Smith, R. L. U. S. Patent 3,928,483, 1975.

(3) Froment, G. F.; Dehertog, W. J. H.; Marchi, A. J. *Catalysis* **1992**, *9*, 2.

(4) (a) Lok, B. M.; Messina, C. A.; Patton, R. L.; Gajek, R. T.; Cannan, T. R.; Flanigen, E. M. *J. Am. Chem. Soc*. **1984**, *106*, 6092. (b) Flanigen, E. M.; Lok, B. M.; Patton, R. L.; Wilson, S. T. In *New Developments in Zeolite Science and Technology*; Murakami, A., Iijima, A., Ward, J. W., Eds.; Elsevier: Amsterdam, 1986; p 129.

(5) (a) Prakash, A. M.; Unnikrishnan, S. *J. Chem. Soc., Faraday Trans.* **1994**, *90*, 2291. (b) Djieugoue, M. A.; Prakash, A. M.; Kevan, L. *J. Phys. Chem. B* **1998**, *102*, 4386. (c) Prakash, A. M.; Kevan, L. *Langmuir* **1997**, *13*, 5341. (d) Prakash, A. M.; Hartmann, M.; Kevan, L. *Chem. Mater*. **1998**, *10*, 932. (e) Djieugoue, M. A.; Prakash, A. M.; Zhu, Z., Kevan, L. *J. Phys. Chem. B* **1999**, *103*, 7277.

(6) Chen, J.; Wright, P. A.; Thomas, J. M.; Natarajan, S.; Marchese, L.; Bradley, S. M.; Sankar, G.; Catlow, R. A.; Gai-Boyes, P. L.; Townsend, R. P.; Lok, C. M. *J. Phys. Chem.* **1994**, *98*, 10216.

(7) Lohse, U.; Loffler, E.; Kosche, K.; Janchen, J.; Parlitz, B. *Zeolites* **1993**, *13*, 549.

(8) Suk, B. H.; Sun, J. K.; Uh, Y. S. *J. Phys. Chem*. **1996**, *100*, 15923.

(9) Bhatia, S. *Zeolite Catalysis: Principles and Applications*; CRC: Boca Raton, FL, 1990; p 166.

(10) (a) Chang, C. D.; Silvestri, A. J. *J. Catal*. **1977**, *47*, 249. (b) Derouane, E. G.; Nagy, J. B.; Dejaifve, P.; VanHooff, J. H. C.; Spekman, B. P.; Vedrine, J. C.; Naccache, C. *J. Catal*. **1978**, *53*, 40.

(11) Chen, D.; Rebo, H. P.; Moljord, K.; Holmen, A. *Ind. Eng. Chem. Res*. **1997**, *36*, 3473.

(12) Chang, C. D. *Catal. Rev. Sci. Eng*. **1984**, *26*, 323.

(13) Simmen, A.; McCusker, L. B.; Baerlocher, Ch.; Meier, W. M. *Zeolites* **1991**, *11*, 654.

(14) Scatterfield, C. N. *Heterogeneous Catalysis in Practice*; McGraw-Hill: New York, 1980; p 151.

(15) Chen, J.; Wright, P. A.; Natarajan, S.; Thomas, J. M. In *Zeolites and Related Microporous Materials: State of the Art*; Weitkamp, J., Karge, H. G., Pfeifer, H., Holderich, W., Eds.; Elsevier: Amsterdam, 1994; p 1731 (*Stud. Surf. Sci. Catal*. **1994**, *84*, 1731).

(16) Wilson, S.; Barger, P. *Microporous Mesoporous Mat.* **1999**, *29*, 117.

(17) Barthomeuf, D. In *Acidity and Basicity of Solids: Theory, Assessment and Utility*; Fraissard, J., Petrakis, L., Eds.; NATO ASI Series C, No. 444; Kluwer Academic: Dordrecht, The Netherlands, 1994; p 375.

(18) Vomscheid, R.; Briend, M.; Peltre, M. J.; Man, D.; Barthomeuf, D. *J. Phys. Chem*. **1994**, *98*, 9614.

(19) Marchi, A. J.; Froment, G. F. *Appl. Catal*. **1991**, *71*, 139.

(20) Zibrowius, B.; Loffler, E.; Hunger, M. *Zeolites* **1992**, *12*, 167.

(21) (a) Martens, J. A.; Janssens, C.; Grobet, P. J.; Bayer, H. K.; Jacobs, P. A. In *Zeolites: Facts, Figures, Future*; Jacobs, P. A., van Santen, R. A., Eds.; Elsevier: Amsterdam, 1989; p 215 (*Stud. Surf. Sci. Catal*. **1989**, *49*, 215). (b) Hasha, D.; de Saldarriaga, L. S.; Hathaway, P. E.; Cox, D. F.; Davis, M. E. *J. Am. Chem. Soc*. **1988**, *110*, 2177.

(22) (a) Kubelkova, L.; Cejka, J.; Nokavoka, J.; Bosacek, V.; Jirka, L.; Jiru, P. In *Zeolites: Facts, Figures, Future*; Jacobs, P. A., van Santen, R. A., Eds.; Elsevier: Amsterdam, 1989; p 1203 (*Stud. Surf. Sci. Catal*. **1989**, *49*, 1203). (b) Karge, H. G.; Laniecki, M.; Ziolek, M.; Onyestyak, G.; Kiss, A.; Kleinschmit, P.; Siray, M. In *Zeolites: Facts, Figures, Future*; Jacobs, P. A, van Santen, R. A., Eds.; Elsevier: Amsterdam, 1989; p 1317 (*Stud. Surf. Sci. Catal*. **1989**, *49*, 1317).

(23) (a) Derouane, E. G. In *Catalysis by Acids and Bases*; Imelik, B., Naccache, C., Coudurier, G., Ben Taarit, Y., Vedrine, J. C., Eds.; Elsevier: Amsterdam, 1985; p 171. (b) Beeckman, J. W.; Froment, G. F. *Ind. Eng. Chem. Fundam*. **1979**, *18*, 245. (c) Beeckman, J. W.; Froment, G. F. *Chem. Eng. Sci*. **1980**, *35*, 805.

(24) Chang, C. D. *Catal. Rev. Sci. Eng*. **1983**, *25*, 1.

(25) Hutchings, G. J.; Themistocleous, T.; Copperthwaite, R. G. *Appl. Catal*. **1988**, *43*, 133.

(26) Gubish, D.; Bandermann, F. *Chem. Eng. Technol*. **1989**, *12*, 155.

(27) Thomas, J. M.; Xu, Y.; Catlow, C. R. A.; Couves, J. W. *Chem. Mater*. **1991**, *3*, 667.

(28) Inui, T.; Phatanasri, S.; Matsuda, H. *J. Chem. Soc., Chem. Commun*. **1990**, 205.

(29) Hartmann, M.; Kevan, L. *J. Chem. Soc., Faraday Trans*. **1996**, *92*, 1429.